Journal of Porphyrins and Phthalocyanines
J. Porphyrins Phthalocyanines 2018; **22**: 1–13
DOI: 10.1142/S1088424618500724

Published at http://www.worldscinet.com/jpp/

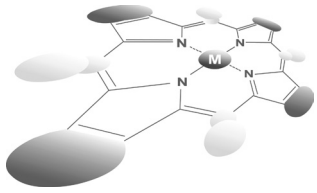

Photophysical properties and photodynamic anti-tumor activity of corrole-coumarin dyads

Fan Cheng[a], Hua-Hua Wang[a], Atif Ali[a], Jaipal Kandhadi[b], Hui Wang*[b], Xiang-Li Wang[a] and Hai-Yang Liu*[a◊]

[a]*Department of Chemistry, Key Laboratory of Functional Molecular Engineering of Guangdong Province, South China University of Technology, Guangzhou, Guangdong 510641, China*
[b]*State Key Laboratory of Optoelectronics Materials and Technologies, Sun-Yat Sen University, Guangzhou, Guangdong 510275, China*

Dedicated to Professor Naisheng Chen on the occasion of his 80th birthday

Received 28 March 2018
Accepted 24 April 2018

ABSTRACT: A new non-conjugated corrole-coumarin dyad and its gallium complex has been synthesized. Photophysical properties of the dyads were tested in two solvents, exhibiting strong solvent effect on the absorption and fluorescence spectra. Absorption spectra of the dyads are a linear combination of the spectra of their corresponding monomers, demonstrating a negligible electronic communication between coumarin and corrole moiety. However, fluorescence emission of coumarin entity in all dyads were quenched significantly as compared to pristine coumarin; this was attributed to intramolecular energy transfer from coumarin to the corrole. Photodynamic anti-tumor tests revealed that gallium corrole-coumarin dyads (**2-Ga**) exhibited good PDT activity towards SiHa cells. After PDT treatment, **2-Ga** could induce apoptosis in SiHa cells, which was associated to cell S phase arrest, collapse of the mitochondrial membrane potential and increase of the intracellular ROS level.

KEYWORDS: corrole, coumarin, gallium, energy transfer, PDT.

INTRODUCTION

Corrole is a tetrapyrrolic macrocycle closely related to porphyrin with a direct pyrrole–pyrrole linkage. It shows a relatively higher fluorescence quantum yield and more intense absorption of red light than its corresponding porphyrin [1]. Corroles have potential applications in the field of photochemical sensors [2, 3], and biomedical devices [4, 5]. Coumarin, also known as 2H-chromen-2-one, is a kind of flavonoid compound of secondary plant metabolites which displays relatively high fluorescent quantum yield. Coumarin derivatives are highly desirable for numerous applications in diverse fields including laser dyes [6], chemical sensor [7], medicinal chemistry [8] and light harvesting [9].

Coumarin-tetrapyrrolic macrocycle conjugates have attracted much interest in the past years [10]. They have potential uses in organic light-emitting diodes (OLEDs) [11, 12], light harvesting [13, 14], fluorescent probes [15, 16] and anti-cancer drugs [17]. Although many coumarin-porphyrin conjugates have been reported [18–21], studies of coumarin–corrole conjugates are scarce. In 2010, Gryko and co-workers reported the first synthesis of corrole-coumarin dyads [13]. They had synthesized a series of conjugated corrole-coumarin dyads using direct condensation of formyl-coumarins and dipyrromethanes [22, 23]. Interestingly, gallium corrole-coumarin dyads could be used as fluorescent probes for anionic or cationic ions [16]. Partly inspired by the lack of literature reporting on corrole-coumarin, and to explore its potential uses in light harvesting and photodynamic anti-cancer therapy, we here wish to report the preparation of a new coumarin–corrole dyad and its gallium complex in which the coumarin unit is

◊SPP full member in good standing

*Correspondence to: Hai-Yang Liu, tel.: +86 020-22236805, fax: +86 020-22236805, email: chhyliu@scut.edu.cn.

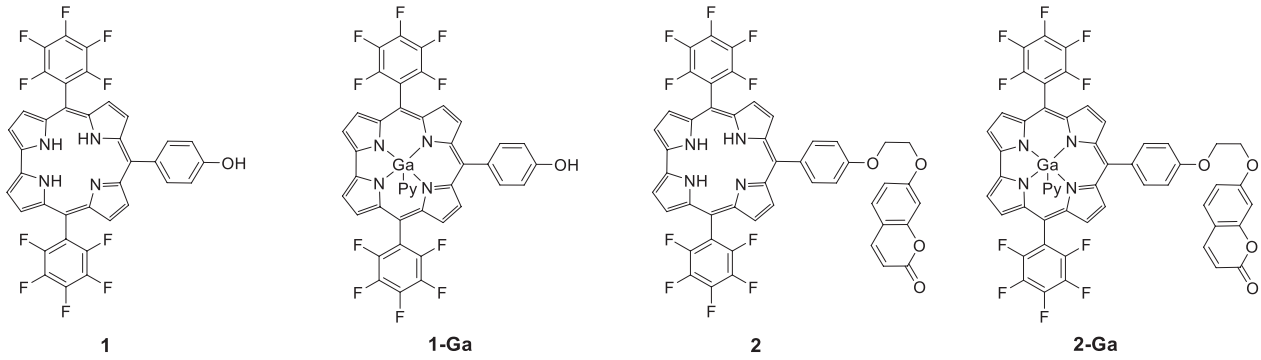

Scheme 1. Cor-Cou dyads and the reference corrole examined in this study

linked to the *para*-position of 10-phenyl group of the corrole (Scheme 1). The compounds were characterized by ^{1}H NMR, ^{19}F NMR, HR-MS, IR and UV-vis spectral (Figs S1–S17). Their photophysical properties, *in vitro* photodynamic anti-cancer activity was also investigated.

RESULTS AND DISCUSSION

Photophysical properties

The UV-vis spectra of the dyads and their reference corroles have been measured in two solvents. As an example, the absorption spectra of free-base dyad **2**, corrole **1** and coumarin in DMF are shown in Fig. 1. The absorption spectrum of the dyad is a linear combination of the spectrum of the corresponding monomers, demonstrating that coumarin was attached with the corrole successfully. Spectral data including maximum absorption wavelength and molar extinction coefficients (ε) are summarized in Table 1. All the dyads showed an intense Soret band located at 418 nm to 429 nm, and Q bands with a lower intensity located at 540–640 nm. These bands characterize the compounds derived from corrole group, while another absorption band around 324 nm corresponds to the coumarin moiety. Interestingly, the Soret band of the free-base dyad was split in DMF (Fig. 1), but a normal Soret band around 429 nm was observed in toluene (Fig. S17). This phenomenon is probably caused by deprotonation of the macrocycle in polar solvents or hydrogen bonding with an internal N–H group inducing solvent dependent changes [24]. From the above observations, we believe the free-base dyad is more solvent dependent, including band shift (Table 1) and Soret band splitting.

The fluorescence spectral studies for dyads along with their monomers were carried out in toluene and DMF (Fig. 2). Spectral data including emission maxima and quantum yields are summarized in Table 1. As an example, the fluorescence emission spectra were recorded at a 420 nm excitation wavelength in toluene, and the Cor-Cou dyad **2** displayed an intense and broad band

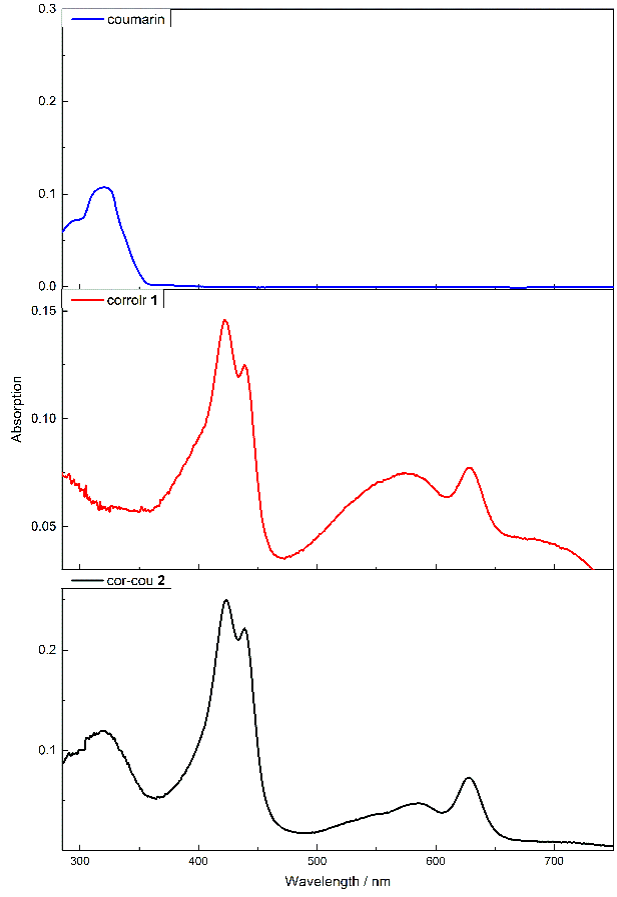

Fig. 1. Absorption spectra of 5 μM complex **1**, **2** and coumarin in DMF

around 641 nm while for **2-Ga** was observed at 618 nm, this fluorescence shift in line with the corresponding Q-band absorption shifts. In addition, an obvious blue shift and fluorescence quenching were observed when the fluorescence spectrum of the dyads was compared with reference corroles (Fig. 2). This behavior suggests that intermolecular interactions are present.

Fluorescence quantum yield measurements were performed with excitation at 535 nm, and the absorbance

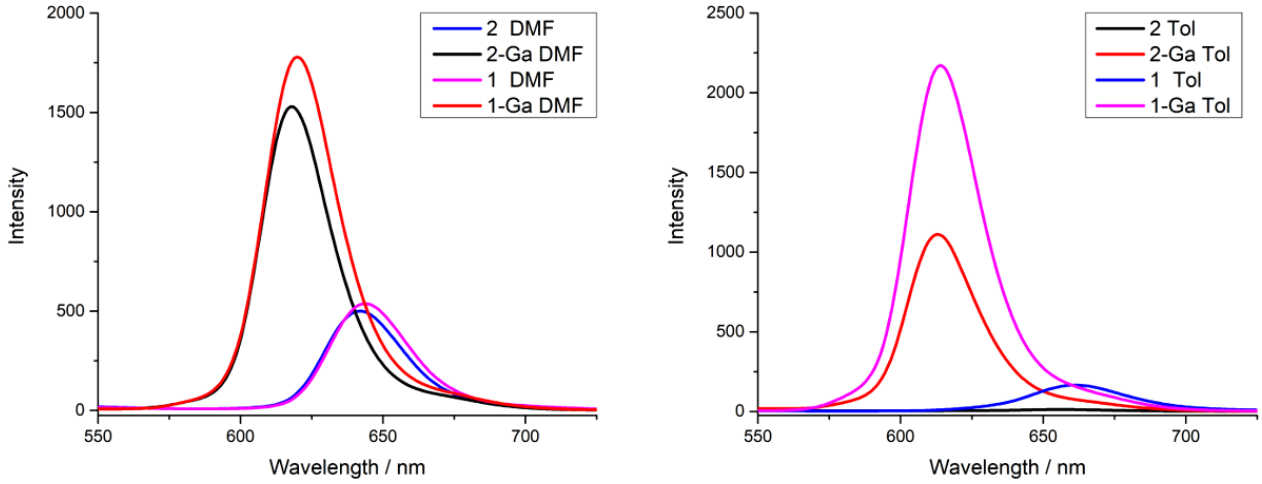

Fig. 2. Fluorescence spectra (λ_{ex} = 420 nm) of 5 μM complex **1**, **1-Ga, 2** and **2-Ga** in DMF and toluene

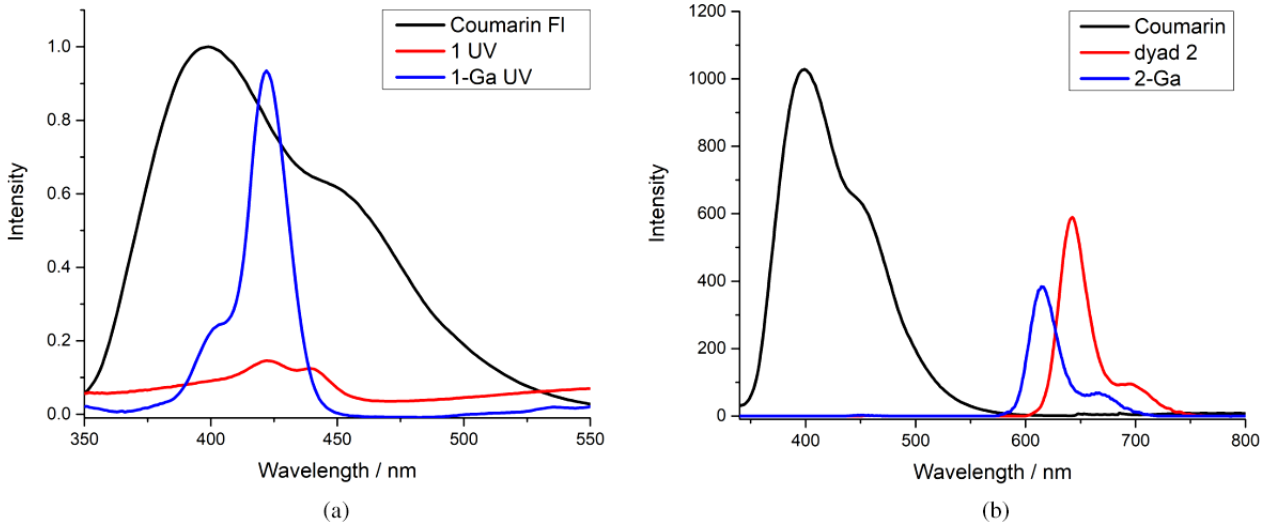

Fig. 3. Comparison of the normalized absorption and fluorescence spectra in DMF at 298K. (a) The absorption spectra of corrole **1** and gallium corrole **1-Ga** are in red and blue respectively and fluorescence spectra of coumarin (λ_{ex} = 320 nm). Note that the folded conformation drawn for the dyads is only to make them fit within the graphs. (b) Normalized fluorescence spectra of 5 μM coumarin and dyads in DMF (λ_{ex} = 320 nm)

of samples at the excitation wavelength was less than 0.1. The fluorescence quantum yield of the gallium dyad was higher than for the free-base dyad. This phenomenon can be explained in part by ring distortion variations [25]. As shown in Table 1, the quantum yields of the dyads are lower than the reference corroles in same solution, suggesting that probably an intramolecular energy transfer or charge transfer occurred. The quenched emission spectra of dyad (λ_{ex} = 320 nm) was compared to that for individual constituent coumarins (between 330–550 nm), and the quenching efficiency was in the range of 96–97%. In addition, an emission band corresponding to the corrole moiety around 600–750 nm was observed (Fig. 3b). A large area overlay of fluorescence spectra of coumarin and absorption spectra of the dyad was also evident (Fig. 3a). The fluorescence quenching demonstrates that an intramolecular fluorescence resonance energy transfer (FRET) occurred from the singlet state of coumarin to corrole.

The fluorescence lifetime of the complexes were measured in two solvents at the excitation wavelength in 405 nm (Table 1). The fluorescence lifetime of the complexes were smaller in DMF as compared to toluene. Furthermore, the fluorescence lifetime of dyad **2** (3.96 ns) was slightly larger than for the reference corrole **1** (3.85 ns). This may be due to weak or negligible electronic interactions from corrole to coumarin in the ground states of the dyads.

Table 1. Photophysical properties of the examined corroles

Compound		Absorption [nm] (ε [$10^3 M^{-1} \cdot cm^{-1}$])					Emission [nm]	ϕ_F	τ [ns]	Φ_Δ
		Soret		Q band						
Cou	toluene	324	—	—	—	—	—	—	0.08	—
	DMF	324	—	—	—	—	393	0.08 [26]	0.19	—
2	toluene	325 (24.3)	429 (29.3)	561 (6.8)	748 (3.0)	—	656	—	3.96	—
	DMF	323 (23.4)	424 (50.0), 439 (44.3)	546 (7.2)	582 (8.6)	628 (14.7)	641	0.14	3.70	0.96
2-Ga	toluene	324 (14.9)	422 (58.4)	576 (7.5)	600 (9.6)	—	613	0.38	2.69	—
	DMF	315 (8.8)	422 (101.1)	576 (6.3)	606 (12.8)	—	618	0.46	2.21	0.28
1	toluene	—	418 (109.8)	563 (15.8)	619 (9.4)	639 (8.3)	662	0.12	3.85	—
	DMF	—	424 (139.1), 439 (118.0)	549 (6.4)	589 (14.1)	631 (41.3)	644	0.18	3.65	0.83
1-Ga	toluene	—	422 (212.5)	576 (20.5)	603 (28.6)	—	615	0.61	2.52	—
	DMF	—	422 (204.3)	578 (17.2)	608 (29.1)	—	621	0.58	2.17	0.68

ε-molar absorption coefficient; stokes shift; Φ_F-fluorescence quantum yield; τ [ns]-fluorescence lifetime; Φ_Δ-singlet oxygen quantum yield.

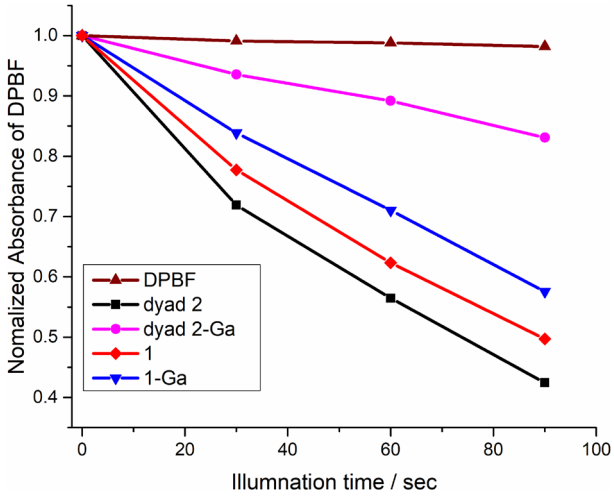

Fig. 4. Plot of change in absorbance of DPBF at 418 nm *vs.* irradiation time in the presence of **1**, **1-Ga, 2** and **2-Ga** in DMF

Singlet oxygen quantum yield

Singlet oxygen generation was determined in DMF using an indirect method by DPBF as singlet oxygen scavenger. A red LED lamp (650 nm) was used as a light source, and absorbance of DPBF at 418 nm decreased in the presence of each complex with increasing illumination time (0–90 s) as shown in Fig. S18. From the slope of the line, we can compare the relative generation of singlet oxygen: the data in Fig. 4 showed that the singlet oxygen of free-base dyad **2** was higher than reference corrole **1**, while the singlet oxygen generated by **2** is greater than for **2-Ga** and singlet oxygen generated by **1** is greater than for **1-Ga**, which is consistent with previous reports [27].

Overall, the results showed the possibility of singlet oxygen generation by Cor-Cou dyads, and corrole-coumarin dyads could promote the singlet oxygen generation. Generation of singlet oxygen is an important step in photodynamic therapy; therefore, the results support that Cor-Cou dyads could be used as potential photosensitizers in photodynamic therapy of cancer.

Cyclic voltammetry

The electrochemical properties of dyad **2** and its gallium complex **2-Ga**, as well as the reference compounds **1** and **1-Ga** were further examined by cyclic voltammetry in DMF at room temperature. The redox data *vs.* the ferrocene/ferrocenium couple (Fc/Fc+) are collected in Table 2. The coordinating metal cation Ga(III) does not show a redox behavior: all the redox processes occur only on the corrole ring and the coumarin. For corrole **1**, two reversible reduction peaks and one oxidation peak were observed. The reversible wave at 0.47 V is due to the redox peak of the internal standard (Fc/Fc+). Other reduction peaks at -0.72 and -1.73 V can be assigned to the reduction of the corrole ring while the oxidation peak (0.21 V) belongs to the oxidation of corrole ring [28]. Compared with corrole, the dyad showed two similar reduction peaks (-1.10 V, -0.65) and an oxidation peak (0.30 V) attributed to the corrole-based reductions and oxidation respectively. Another reduction peak at -1.83 V was assigned to reduction of coumarin. The reduction potentials of the dyad are shifted to a more positive state, indicating that the Cor-Cou dyad is easier to reduce and harder to oxidize compared to its corresponding monomers.

In case of gallium dyad, the first reduction peak (-1.53) should be assigned to reduction of the corrole ring, and the second reversible reduction peak (-1.84V) should be assigned to coumarin-based reductions. No oxidation peak could be observed in the cyclic voltammogram

Table 2. Redox potentials of porphyrins (V *vs.* $Ag/AgNO_3$; Pt electrode as a working electrode; TBAP 0.1 M, DMF)

	E_{red3}/V	E_{red2}/V	E_{red1}/V	Fc/Fc^+	E_{ox1}/V
Coumarin	-1.92	—	—	0.47 (0.09)	1.23
1	—	-1.73 (0.15)	-0.72 (0.11)	0.47 (0.08)	0.21 (0.06)[a]
1-Ga	—	-1.47 (0.15)	—	0.53 (0.09)	—
2	-1.83	-1.10	-0.65	0.49 (0.07)	0.30
2-Ga	-1.84	-1.53	—	0.49 (0.09)	—

[a]Reversible redox. $\Delta E = E_{pa} - E_{pc}$ in brackets.

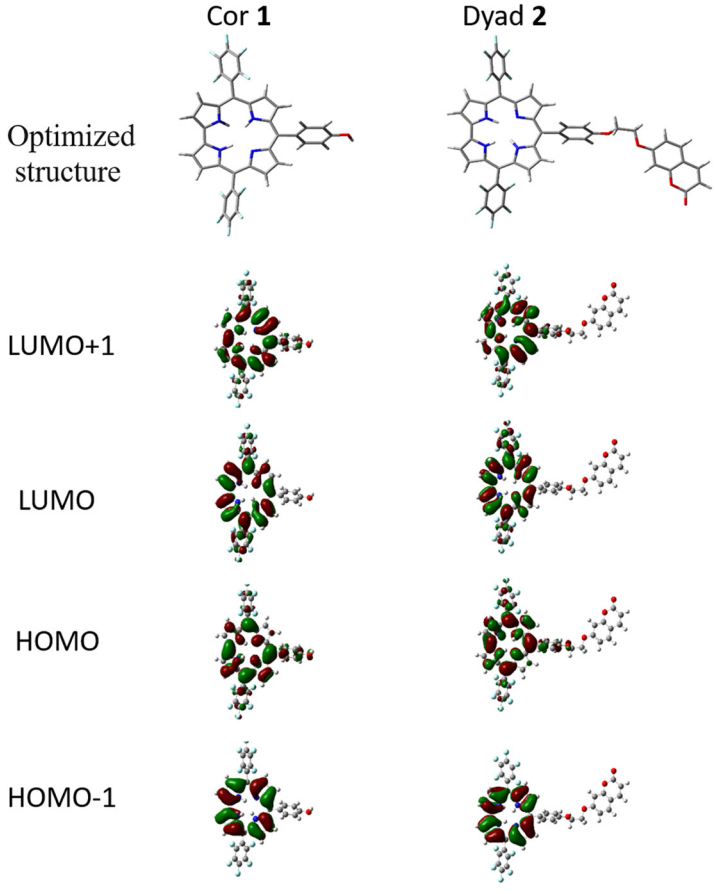

Fig. 5. DFT optimized geometry of dyads and frontier molecular orbitals of complex **1**, **2** optimized at the B3LYP/6-31G (d,p) level

of the gallium dyad. A similar phenomenon was also observed for monomer gallium corrole **1-Ga**.

Theoretical studies

Detail of the DFT calculations shown in the experimental section. Calculated optimized geometry shows that the non-conjugated arm does not influence the structure of corrole molecule, and the gallium corrole appears more planar than free-base corrole (Fig. S19). Calculated distribution patterns of the free-base dyad are shown in Fig. 5, where it can be seen that the frontier molecular orbitals HOMO, HOMO-1, LUMO and LUMO+1 orbital of the complex are all localized on the corrole dye but not on the substituent. However, HOMO-2 is localized on the coumarin molecule, including the *meso* linker group, as well as the LUMO+2 orbital (data not shown). Similar results were obtained for the gallium complexes (Fig. S19).

The TD-DFT calculated spectra of the dyads in the two solvents are presented in Fig. 6. With toluene as the solvent, the calculated Q band was located at 626 nm, which corresponds to the HOMO → LOMO (90%). The intensive Soret band composed of two transitions with absorption maxima at 439 nm and 393 nm, represents the HOMO-1 → LUMO (40%), HOMO → LUMO+1 (55%) and HOMO-1 → LUMO+1 (45%) and HOMO-2 → LUMO (17%) transfers. Another less intensive band at 300–400 nm with absorption maxima at 344 nm, represents HOMO → LUMO+3 (74%). Most of these transitions take place on the corrole part of the molecule, with only HOMO-2 → LUMO participation of the coumarin part. This suggests a weak charge-transfer (CT) character from the corrole to the coumarin part. Similar results were observed in DMF: the calculated Q band is formed by some transitions with absorption maxima at 668 nm, which corresponds to HOMO → LUMO (96%). Two intensive Soret bands were observed at 472 nm, representing the HOMO → LUMO+1 (60%), HOMO-1 → LUMO (38%) and at 413 nm, corresponding to HOMO-1 → LUMO+1 (66%) HOMO-2 → LUMO (14%). Another band at 318 nm corresponds to HOMO-2 → LUMO+2 (83%) and HOMO-3 → LUMO+2 (13%). The calculated UV-vis spectra of the free-base dyads showed an obvious shift in two solvents, consistent with the experimental results. Furthermore, TD-DFT calculated spectra of the gallium dyads are presented in Fig. S20,

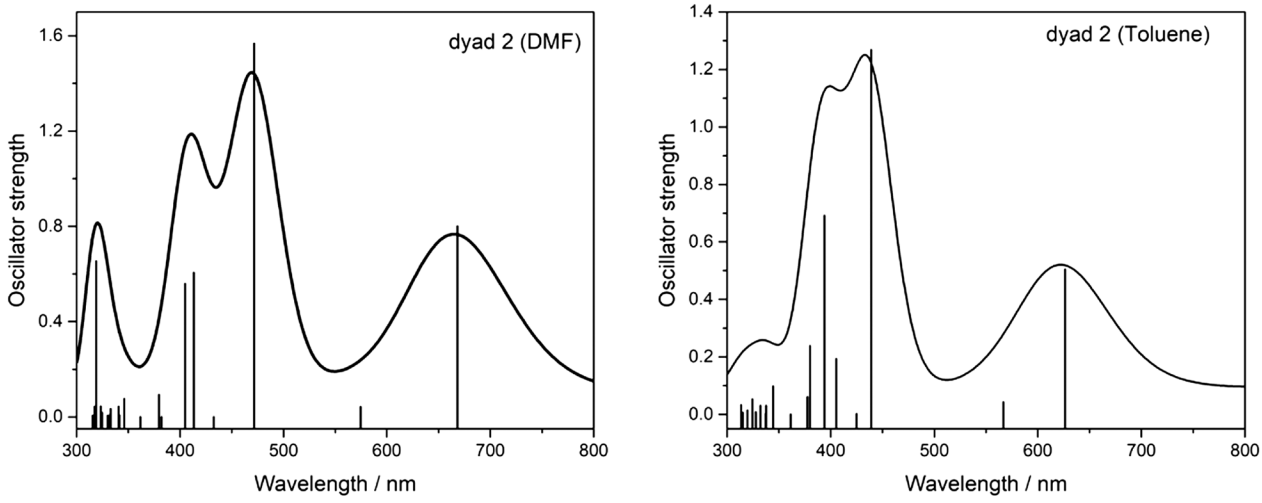

Fig. 6. Computed TD-DFT spectra of dyad **2** with inclusion of DMF or toluene as solvent

Table 3. The IC_{50} (μM) values of corrole and dyads towards Bel-7402, A549 and SiHa cell lines

Com	BEL-7402		A549		SiHa	
	dark	light	dark	light	dark	light
2	>100	>100	>100	>100	>100	>100
2-Ga	>100	35.4 ± 1.4	>100	75.4 ± 1.1	>100	15.8 ± 1.2
1	29.1 ± 2.3	1.1 ± 0.4	>100	0.7 ± 0.1	>100	3.5 ± 0.8
1-Ga	8.3 ± 1.1	0.2 ± 0.01	1.6 ± 0.1	0.2 ± 0.04	11.4 ± 0.1	0.1 ± 0.01

Results represent means ± SD of three independent experiments. Light dose = 22 $J \cdot cm^{-2}$.

proving the weak charge-transfer (CT) character from the gallium corrole to the coumarin.

Cytotoxicity assay

The light-induced antitumor activities of the dyads were investigated *in vitro* by the MTT method, using three tumor cell cultures for study. A red LED lamp (650 nm) was used as a light source, and light wavelengths used were within the range of effective PDT wavelengths (600–800 nm); the results are listed in Table 3. Reference corrole **1** showed lower toxicity in the dark; after exposure to the light, the half-maximal inhibitory concentration (IC_{50}) value even dropped to 0.7 μM towards A549 cells. However, the target compound (**2**) showed no apparent toxicity even at a high concentration of 100 μM in either dark or light. The above research indicates that the corrole-coumarin dyad **2** enhanced the singlet oxygen quantum yield compared to the reference corrole. Unfortunately this enhancement effect did not work in antiproliferative activities of tumor cells. This may be explained by optimizing the structure of DFT calculation. The increased π–π stacking leads to self-aggregation of either corrole or coumarin, and we also observed the poor solubility of the free-base dyad compared with the free-base corrole, which may hinder the compound's ability to enter into cells smoothly.

Gallium corroles can increase the cytotoxicity and showed brighter red fluoresence compared with free-base corroles in our study. The reference gallium corrole showed stronger cytotoxicity in both dark and light compared with the corrole. The target Ga(III)corrole-coumarin complex showed low cellular toxicity in the dark, with an IC_{50} value over 100 μM, and the IC_{50} exhibited significant reduction after exposure to red light (650 nm), especially towards SiHa cells, where the phototoxicity increased more than 6 times compared with dark toxicity. Despite the fact that the dyads did not show cytotoxicity as expected, this data still provides a case that gallium complexes may be good candidates for antitumor therapy. Next, SiHa cells were taken as an example to investigate the antitumor mechanism of gallium corrole-coumarin dyads.

Intracellular location

It is well known that intracellular uptake is an important property of a photosensitizer. DAPI was used as the

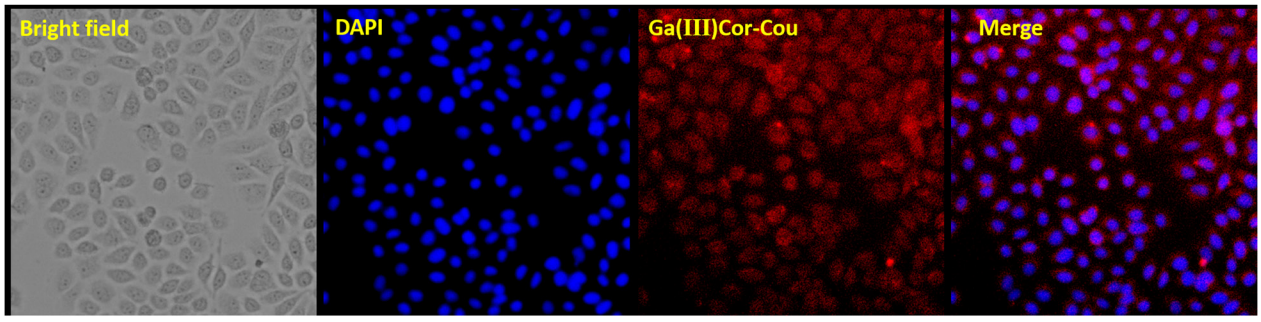

Fig. 7. Cellular uptake of SiHa cells with exposure to 30 μM **2-Ga** (up red channel) for 24 h at 200× magnification

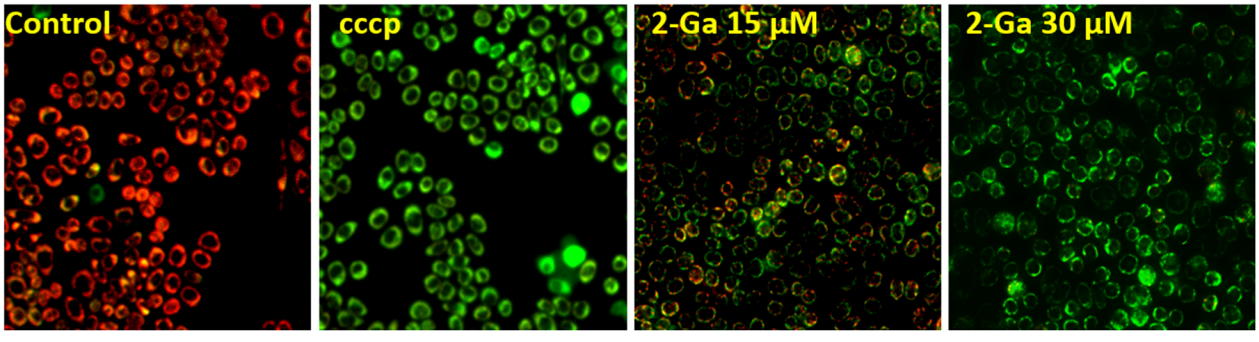

(a)

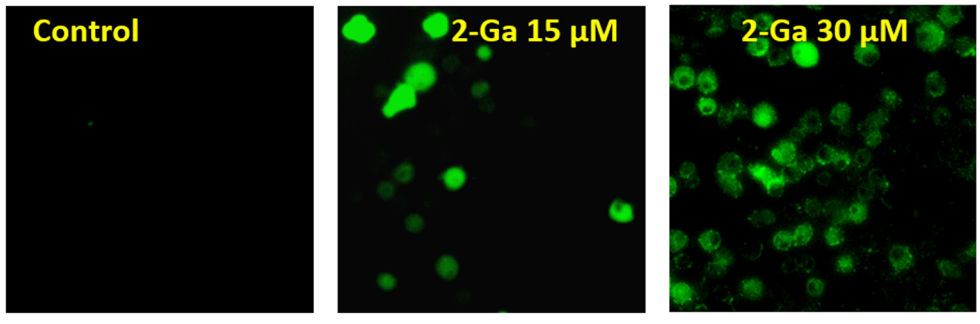

(b)

Fig. 8. (a) Assay of SiHa cells mitochondrial membrane potential with JC-1 as fluorescence probe staining method. (b) Intracellular ROS was detected in SiHa cells. All were treated with red light (650 nm) for 2 h and incubated for 24 h at 200× magnification

nuclear staining dye to evaluate the intracellular location and thereby to further investigate the mechanism of PDT action. SiHa cells were treated with 30 μM dyad **2-Ga** for 24 h, Fig. 7 shows that the bright red fluorescence of **2-Ga** can be uptaken by SiHa cells without the help of an internalizing protein. The merged spectrum shows that the red fluorescence signals from **2-Ga** accumulated not only in the cytoplasm but also in the nucleus of the SiHa cells after incubation for 24 h.

Effects on mitochondrial dysfunction and ROS generation

The cell-permeant dye, JC-1, was used to monitor any loss of mitochondrial membrane potential (MMP, Ψm), since decreased MMP has been implicated as an early event in apoptotic cells. Dye JC-1 shows red fluorescence in its aggregated form and exists as a green-emissive monomer after loss of the mitochondrial membrane potential. Carbonyl cyanide *m*-chlorophenyl hydrazone (CCCP), a mitochondrial electron transport chain inhibitor, was used as a positive control. Figure 8a shows that the SiHa cells lost the MMP completely after treatment with CCCP. SiHa cells exposed to gallium dyads and then treated with a red light (650 nm) for 2 h showed reduced red fluorescence intensity with a concomitant increase in the green signal. Furthermore, there was an obvious increase of green fluorescence as the concentration of **2-Ga** increased from 15 to 30 μM. All of the above suggest that **2-Ga** can reduce the MMP of SiHa cells during the apoptosis process.

Mitochondria are an important intracellular source of reactive oxygen species (ROS) [29]. To further explore the mechanism of the examined dyads for anti-cancer cells, we also explored intracellular ROS levels of SiHa cells after exposure to **2-Ga**, using an oxidation-sensitive fluorescent probe DCFH-DA, to measure the ability of **2-Ga** to generate ROS. As shown in Fig. 8b, the green fluorescence which reflects the level of intracellular ROS, was difficult to observe in the control group. In contrast, for SiHa cells exposed to gallium dyads and then treated with LED light (650 nm) for 2 h and incubated for 24 h, the intensity of the green fluorescence was brighter than that of the control group. Furthermore, the green fluorescence became progressively brighter when the concentration of gallium dyad was increased. Altogether, according to the observed loss of mitochondrial potential, dyad **2-Ga** was able to increase ROS levels and eventually triggered apoptotic cell death.

Comet assay

DNA fragmentation is a hallmark of apoptosis, mitotic catastrophe or both [30]. Single cell gel electrophoresis (comet assay) in an agarose gel matrix was used to study DNA fragmentation. As shown in Fig. 9, in the control, SiHa cells failed to show a comet-like appearance. Treatment of SiHa cells with 15 μM of complex showed statistically significant and well-formed comets, with the length of the comet tail representing the extent of DNA damage. These results clearly indicate that **2-Ga** indeed induced DNA fragmentation, which is further evidence of apoptosis.

Cell-cycle assay

In the following study, the **2-Ga** complex was examined for its effect on cell cycle progression of SiHa cells by flow cytometry. As shown in Fig. 10, the complex led to an accumulation of cells in the S phase, from 18.10% to 45.64%, with a concomitant decrease of cells in the G1 and G2/M phase cells. Furthermore, the apoptotic cells increased from 0.24% to 4.89% after exposure to **2-Ga**. These results imply that dyad **2-Ga** induces cell cycle arrest at the S phase, probably through induction of apoptosis.

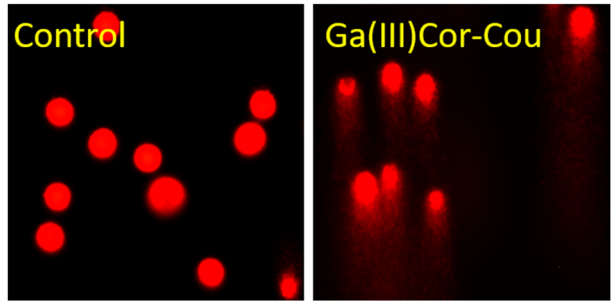

Fig. 9. Comet assay of EB-stained control and 15 μM of complexes 2-Ga treated SiHa cancer cells. Red well-formed comets were observed

EXPERIMENTAL

Materials and methods

All reagents were purchased from commercial sources and used without further purification unless otherwise mentioned. UV-vis absorption spectra were measured on a Hitachi 3900H spectrophotometer in 1 cm optical path length quartz cells at room temperature. Fluoresce emission spectra were measured using a Hitachi F-4500 fluorescence spectrophotometer. Intracellular location

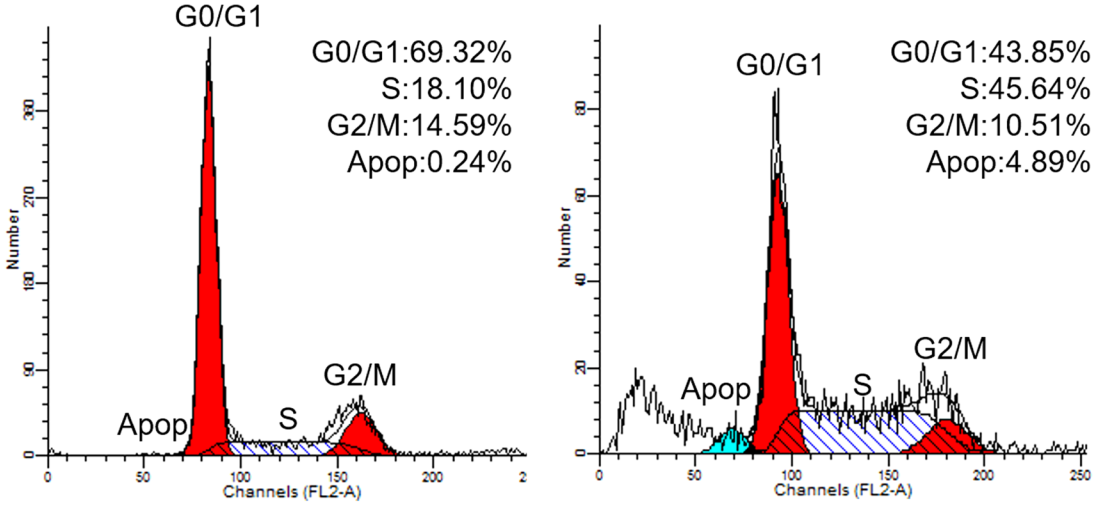

Fig. 10. Cyclic progression of SiHa cells treated with 15 μM **2-Ga**. Cells were harvested, fixed with 70% ethanol, and stained with propidium iodide (PI). The cellular DNA content was then determined by flow cytometry analysis

was visualized using an Axio Observer Z1 fluorescence microscope. HR-MS spectra were recorded on an Esquire HCT PLUS mass spectrometer. ^{1}H NMR spectra were recorded on a 400 MHz spectrometer in $CDCl_3$ or DMSO-d_6 solution.

All biological experiments were prepared using Ultrapure MilliQ water. A red LED lamp (650 nm) was used as the light source. The distance between the light source and the surface of the sample was kept constant (10 cm) in all experiments. LED irradiance was measured using a TES-1330A luxmeter (TES, Taiwan) at the plate surface. The irradiance dose used for the present work is 3 mw·cm^{-2}, and the light reached to 22 J·cm^{-2} after irradiation for 2 h. Cell lines of human hepatocellular carcinomas (Bel-7402), human lung cancer (A549) and human cervical cancer (SiHa) were purchased from the American Type Culture Collection. Cancer cells were cultured in RPMI 1640, with the supplement of 10% fetal bovine serum (FBS; Gibco, US).

Fluorescence quantum yield

Luminescence quantum yields (Φ_F) were measured in dilute *N*,*N*-Dimethylformamide (DMF) solutions with an absorbance below 0.1 by using Equation 1 where A (λ) is the absorbance at the excitation wavelength (λ), *n* is the refractive index, and *I* is the integrated luminescence intensity. Subscripts "*r*" and "*s*" stand for reference and sample, respectively.

$$\frac{\Phi_{Fs}}{\Phi_{Fs}} = \frac{A_r(\lambda)}{A_s(\lambda)} \times \frac{I_s}{I_r} \times \frac{n_s^2}{n_r^2} \quad (1)$$

5,10,15,20-Tetraphenylporphyrin (TPP) in aerated toluene was used as a standard with $\Phi_F = 0.11$ [31].

Fluorescence lifetime

Fluorescence lifetimes of porphyrin and dyads were measured by time-correlated single-photon counting using a FLSP920 Combined Fluorescence Lifetime and Steady State Spectrometer (Edinburgh Instruments) with a pulse diode laser EPL 405 (Edinburgh Instruments) with spectral full-width half maximum of 405 ± 10 nm and pulse width 58.8 ps at a 10 MHz repetition rate. Fluorescence decays of porphyrin and dyads were observed at 650 nm. Highly dilute colloidal silica (Ludox) in water as a scattered solution was used to acquire the instrument response function (IRF). Data acquisition took place until a maximum count in a single channel reached at least 10^4. All experiments were performed at room temperature for air-equilibrated solutions using quartz cuvettes.

Fluorescence lifetimes of coumarin were measured with a laser excitation wavelength at 310 nm, and fluorescence decays were observed at 410 nm.

Singlet oxygen quantum yield

For the singlet oxygen generation experiment, an aerated solution of 1,3-diphenylisobenzofuran (DPBF) (20 μM) and photosensitizer (0.5 μM) in DMF (3 mL) was irradiated at 650 nm under a LED lamp (650 nm) at 25 °C for 60 s intervals. Reaction of DPBF with $^1O_2$ was monitored by the decreasing intensity of the absorption band at 418 nm over time.

Theoretical calculations

Full geometry optimization computations of the dyads porphyrin-coumarin dyads were carried out with the DFT-B3LYP method using the 6-31G (d,p) basis set and for the Ga atom, the lanl2DZ basis set. Frequency analysis confirmed that the obtained geometries are genuine global minimum structures. All calculations were performed with the Gaussian G09 package [32].

Cyclic voltammetry

All cyclic voltammograms (CV) were performed in DMF solution containing 0.1 M tetrabutylammonium perchlorate (TBAP) and complexes (1 mM) under nitrogen atmosphere at ambient temperature. The scan rate was 100 mV/s. A three-electrode system consisting of a glassy carbon working electrode, a platinum wire counter electrode and a saturated Ag/$AgNO_3$ electrode as the reference electrode was employed. The Ag/$AgNO_3$ electrode contained 1 M TBAP in DMF. Half-wave potentials ($E_{1/2}$) for reversible or quasi-reversible redox processes were calculated as $E_{1/2} = (E_{pa} + E_{pc})/2$, where E_{pa} and E_{pc} represent the anodic and cathodic peak potentials, respectively. The $E_{1/2}$ value for the ferrocene couple under these conditions was 0.47 V.

Cytotoxicity assays

An MTT assay was carried out using 5×10^3 cells in 100 μl of medium seeded on 96-well plates and grown overnight at 37 °C in a 5% CO_2 incubator. Serial dilutions of the complex ranging from 0.2–100 μM in DMSO were added to the monolayer. The plates were incubated at normal condition for 48 h. The cultures were assayed after the addition of 20 μl of 5 mg·mL^{-1} MTT and incubation for 4 h at 37 °C. Finally, the MTT-containing medium was aspirated, and the buffer (100 μL) containing DMSO (50%) and sodium dodecyl sulfate (20%) was added to solubilize the MTT formazan. The optical density of each well was measured with a microplate spectrophotometer at a wavelength of 490 nm. The IC_{50} values were determined by plotting the percentage of cell viability *vs*. concentration on a logarithmic graph and reading off the concentration at which 50% of cells remained viable relative to the control. Each experiment was repeated at least three times to obtain the mean values.

Intracellular location

A549 cells were placed in 24-well micro assay culture plates (4×10^4 cells per well) and grown overnight at 37 °C in a 5% CO_2 incubator. Then the test compounds were added to the wells. The plates were incubated at 37 °C in a 5% CO_2 incubator for 24 h. Upon completion of the incubation, the wells were washed three times with PBS. After removing the culture medium, the cells were stained with DAPI and imaged by fluorescence microscopy.

Mitochondrial membrane potential assay

SiHa cells in a growth medium (2×10^5 cells/well) were seeded on a sterilized coverslip in six-well plates and grown overnight at 37 °C in a 5% CO_2 incubator. **2-Ga** was added to the wells and incubated at 37 °C in 5% CO_2 for 4 h, then cells were exposed to the red light for 2 h. After incubation for 18 h, the cells were incubated for 20 min with 1 mg/mL of 5,5′,6,6′-tetrachloro-1,1′,3,3′-tetraethyl-imidacarbocyanine iodide (JC-1) in culture medium at 37 °C in the dark. The cell pellets were suspended in PBS and then imaged under a fluorescence microscope.

Reactive oxygen species (ROS) level detection

SiHa cells were seeded into six-well plates at a density of 2×10^5 cells per well and incubated for 24 h at 37 °C in 5% CO_2. The medium was removed and replaced with medium containing **2-Ga**. After incubation at 37 °C in 5% CO_2 for 4 h, the cells were irradiated for 2 h. Followed by incubation for 18 h, the medium was removed. The fluorescent dye 2′,7′-dichlorodihydrofluorescein diacetate (DCHF-DA, 10 μM) was added to the medium and the cells were imaged by fluorescence microscopy.

Cell cycle arrest studies

SiHa cells were seeded into six-well plates at a density of 1×10^6 cells per well and incubated for 24 h. The cells were cultured in RPMI 1640 supplemented with 10% of FBS and incubated at 37 °C and 5% CO_2. The medium was removed and replaced with medium containing complex **2-Ga** (15 μM). Then the cells were treated with red light for 2 h and incubated for 24 h at 37 °C. After incubation, the cell layer was trypsinized and washed with cold PBS and fixed with 70% ethanol. 20 μL of RNAse (0.2 mg/mL) and 20 μL of propidium iodide (0.02 mg/mL) were added to the cell suspensions and the mixtures were incubated at 37 °C for 30 min. The samples were then analyzed with a FACSCalibur flow cytometer.

Comet assay

DNA damage was investigated by means of a comet assay. The control SiHa cells were incubated for 24 h. The experimental group was incubated with 15 μM of complex treated with red light 2 h and then incubated for 24 h at 37 °C. The cells were harvested by a trypsinization process at 24 h. A total of 100 μL of 0.5% normal agarose in PBS was dropped gently onto a fully frosted microslide, covered immediately with a coverslip, and then placed at 4 °C for 10 min. The coverslip was removed after the gel had set. 50 μL of the cell suspension (200 cells/μL) was mixed with 50 μL of 1% low-melting agarose preserved at 37 °C. A total of 100 μL of this mixture was applied quickly on top of the gel, coated over the microslide, covered immediately with a coverslip, and then placed at 4 °C for 10 min. The coverslip was again removed after the gel had set. A third coating of 50 μL of 0.5% low melting agarose was placed on the gel and allowed to set at 4 °C for 15 min. After solidification of the agarose, the coverslips were removed, and the slides were immersed in an ice-cold lysis solution (2.5 M NaCl, 100 mM EDTA, 10 mM Tris, 90 mM sodium sarcosinate, NaOH, pH 10, 1% Triton X-100 and 10% DMSO) and placed in a refrigerator at 4 °C for 2 h. All of the above operations were performed under low light conditions to avoid additional DNA damage. The slides, after removal from the lysis solution, were placed horizontally in an electrophoresis chamber. The reservoirs were filled with an electrophoresis buffer (300 mM NaOH, 1.2 mM EDTA) until the slides were immersed in it, and the DNA was allowed to unwind for 30 min in an electrophoresis solution. Then electrophoresis was carried out at 25 V and 300 mA for 20 min. After electrophoresis, the slides were removed, washed three times in a neutralization buffer (400 mM Tris, HCl, pH 7.5). Nuclear DNA was stained with 20 μL of EtBr (20 μg/mL) in the dark for 20 min. The slides were washed in chilled distilled water for 10 min to neutralize the excess alkali, air-dried and scored for comets by fluorescence microscopy.

Synthetic procedures

The reference corrole **1** and **1-Ga** with mono-hydroxyl groups were synthesized according to the general method [33, 34].

1. ^{1}H NMR (400 MHz, $CDCl_3$, Me_4Si): δ 9.11 (d, *J* = 4.3 Hz, 2H, pyrrole–*H*), 8.71 (s, 4H, pyrrole–*H*), 8.57 (d, *J* = 4.2 Hz, 2H, pyrrole–*H*), 8.02 (d, *J* = 8.3 Hz, 2H, Ph), 7.14 (d, *J* = 8.0 Hz, 2H, Ph). ^{19}F NMR (376 MHz, $CDCl_3$) δ -137.86 (dd, *J* = 23.6, 7.9 Hz), -152.90 (t, *J* = 20.9 Hz), -161.80 (dt, *J* = 23.1, 7.6 Hz). IR (KBr) ν_{max}, cm^{-1}: 3328–3508 (N–H, O–H), 1649, 1606, 1521, 1494, 1434, 1282, 1176, 1159, 1058, 982, 928, 847, 795, 758.

1-Ga. ^{1}H NMR (400 MHz, DMSO, Me_4Si): δ 9.77 (s, 1H, –O*H*), 9.30 (s, 2H, pyrrole–*H*), 9.11–8.64 (m, 6H, pyrrole-*H*), 8.54 (d, *J* = 6.8 Hz, 2H, pyridine–*H*), 7.96 (d, *J* = 7.0 Hz, 2H, Ph), 7.77 (t, *J* = 6.7 Hz, 1H, pyridine–*H*), 7.36 (d, *J* = 4.5 Hz, 2H, pyridine–*H*), 7.19 (d, *J* = 7.2 Hz, 2H, Ph). ^{19}F NMR (376 MHz, DMSO) δ -139.06 (d, *J* = 25.9 Hz), -155.48 (t, *J* = 22.2 Hz), -163.29 (dd, *J* = 34.5,

13.9 Hz). IR (KBr) ν_{max}, cm^{-1}: 3436 (O–H), 1612, 1519, 1492, 1332, 1290, 1234, 1168, 1060–1035 850, 793, 760, 704–692.

Synthesis of (4-(2-coumarin-7-oxy)ethoxy) benzaldehyde

The aldehyde was synthesized as shown in Scheme 1. First, 4-hydroxybenzaldehyde (5.0 g, 40.9 mmol) was reacted with 1,2-dibromoethane (11.5 g, 61.4 mmol), dissolved in dry DMF (20 mL), then K_2CO_3 was added and the mixture was stirred under room temperature for 24 h. The progress of the reaction was monitored by thin-layer chromatography (TLC). After the reaction, the product was washed several times with dichloromethane and saturated salt water, and the organic phase was collected. The crude product was purified by silica gel chromatography (100–200 mesh) with DCM/hexane (1:2) used as the eluent, and 4-(2-bromoethoxy)benzaldehyde was obtained as a pale yellow solid (yield 76%). Second, 4-(2-bromoethoxy)benzaldehyde (5.0 g, 21.8 mmol) was reacted with 7-hydroxycoumarin (7.1 g, 43.7 mmol), K_2CO_3 was added dissolved in dry DMF, reflux reacted for 24 h, then the product was washed several times with dichloromethane and water, and the organic phase was collected. The crude product was purified by silica gel chromatography (100–200 mesh) with DCM/hexane (1:2) used as the eluent. (4-(2-coumarin-7-oxy)ethoxy) benzaldehyde was obtained as a pale yellow solid (yield 61%).

4-(2-*Bromoethoxy*)*benzaldehyde.* ^{1}H NMR (400 MHz, $CDCl_3$, Me_4Si): δ 9.85 (s, 1H, –C*H*O), 7.80 (d, *J* = 8.6 Hz, 2H, Ph), 6.97 (d, *J* = 8.5 Hz, 2H, Ph), 4.35 (dd, *J* = 21.7, 15.6 Hz, 2H, –CH_2), 3.63 (t, *J* = 6.1 Hz, 2H, –CH_2).

(4-(2-*Coumarin*-7-*oxy*)*ethoxy*)*benzaldehyde.* MS (HR-MS): m/z 333.0740 (calcd for $[M + Na]^+$ 333.0733); ^{1}H NMR (400 MHz, $CDCl_3$, Me_4Si): δ 9.90 (s, 1H, –C*H*O), 7.86 (d, *J* = 8.2 Hz, 2H, Ph), 7.64 (d, *J* = 9.5 Hz, 1H, cou–*H*), 7.39 (d, *J* = 8.3 Hz, 1H, cou–*H*), 7.06 (d, *J* = 8.3 Hz, 2H, Ph), 6.89 (d, *J* = 10.2 Hz, 2H, cou–*H*), 6.27 (d, *J* = 9.5 Hz, 1H, cou–*H*), 4.43 (d, *J* = 4.2 Hz, 4H, –CH_2–CH_2). ^{13}C NMR (101 MHz, $CDCl_3$) δ 190.83 (s), 163.52 (s), 161.74 (s), 161.13 (s), 155.97 (s), 143.40 (s), 132.15 (s), 130.61 (s), 129.04 (s), 115.04 (s), 113.69 (s), 113.12 (d, *J* = 4.6 Hz), 101.77 (s), 66.94 (s), 66.61 (s).

Synthesis of dyad 2

5-(pentafluorophenyl) dipyrromethane (5F-DPM) was prepared according to previously published methods [35]. Synthesis of **2**: 5-(pentafluorophenyl) dipyrrylmethane (0.25 g, 0.8 mmol) and (4-(2-coumarin-7-oxy)ethoxy) benzaldehyde (0.13 g, 0.4 mmol) were dissolved in dichloromethane (DCM, 10 mL), mixed in 6 μL THF, stirred for 5 h at room temperature. Then 12 μL trimethylamine, 40 mL DCM and 0.18 g (0.8 mmol) DDQ were added and the mixture was stirred at room temperature for 1 h. DDQ was removed through the silica gel chromatography (100–200 mesh) with DCM to provide the crude product. The crude product was purified by silica gel chromatography (300–400 mesh) with DCM/hexane (1:1) used as the eluent, and **2** was obtained as a dark violet solid after recrystallization from DCM and hexane (yield 29%).

2. MS (HR-MS): m/z 911.1716 (calcd for $[M]^+$ 911.1711); ^{1}H NMR (400 MHz, DMSO, Me_4Si): δ 9.21 (s, 2H, pyrrole–*H*), 8.94 (s, 2H, pyrrole–*H*), 8.72 (s, 2H, pyrrole–*H*), 8.61 (s, 2H, pyrrole–*H*), 8.04 (d, *J* = 12.5 Hz, 3H, Ph, cou–*H*), 7.71 (d, *J* = 7.6 Hz, 1H, cou–*H*), 7.43 (s, 2H, cou–*H*), 7.16 (d, *J* = 24.0 Hz, 2H, Ph), 6.34 (d, *J* = 8.8 Hz, 1H, cou–*H*), 4.64 (s, 4H, –CH_2–CH_2). ^{19}F NMR (376 MHz, DMSO) δ -139.59 (d, *J* = 22.7 Hz), -154.82 (t, *J* = 21.4 Hz), -162.88 (t, *J* = 21.2 Hz). IR (KBr) ν_{max}, cm^{-1}: 3437 (N–H), 2927–2850 (aliphatic–CH), 1739 (C=O), 1650, 1608, 1521, 1495, 1426, 1283, 1248–1231 (C–O), 1178, 1159, 1124 (C–O), 1059, 984, 930, 837, 797, 758.

Synthesis of gallium dyad 2-Ga

The corrole-coumarin dyad **2** (30.0 mg, 0.033 mmol) and Gallium(III) chloride (58 mg, 0.33 mmol) were dissolved in pyridine (10 mL), reflux stirred under argon atmosphere for 2 h. After the reaction was complete, the mixture was cooled to room temperature, the solvent was evaporated and the residue was dissolved in DCM, filtered, dried, and evaporated. The crude product was purified by silica gel chromatography (200–300 mesh) with DCM/pyridine (100:1) used as the eluent. A red fraction was collected. The solvent was evaporated under vacuum and **2-Ga** was obtained as a purple-red solid after recrystallization from DCM and hexane in an 81% yield.

2-Ga. MS (HR-MS): m/z 999.0549 (calcd for [M – pyridine + Na] 999.0551); ^{1}H NMR (400 MHz, DMSO, Me_4Si): δ 9.31 (d, *J* = 3.6 Hz, 2H, pyrrole–*H*), 8.99 (s, 2H, pyrrole–*H*), 8.90 (s, 2H, pyrrole–*H*), 8.72 (d, *J* = 4.4 Hz, 2H, pyrrole–*H*), 8.56 (s, 2H, pyridine–*H*), 8.07 (dd, *J* = 19.5, 8.6 Hz, 3H, Ph), 7.86–7.65 (m, 2H, cou–*H*, pyridine–*H*), 7.56–7.29 (m, 4H, cou–*H*, pyridine–*H*), 7.20 (s, 1H, Ph), 7.13 (d, *J* = 8.8 Hz, 1H, cou–*H*), 6.34 (d, *J* = 9.6 Hz, 1H, cou–*H*), 4.65 (s, 4H, –CH_2–CH_2). ^{19}F NMR (376 MHz, DMSO) δ -139.07 (dd, *J* = 25.7, 6.0 Hz), -155.45 (t, *J* = 21.9 Hz), -163.00 – -163.71 (m). IR (KBr) ν_{max}, cm^{-1}: 3448 (O–H), 2929–2858 (aliphatic–CH), 1735 (C=O), 1610, 1519, 1492, 1332, 1290, 1230, 1122 (C–O), 1031, 986, 957, 837, 795, 762, 692.

CONCLUSIONS

In summary, we have synthesized a new corrole-coumarin dyad and its gallium complex. Intramolecular energy transfer from the coumarin to the corrole moiety was observed after excitation of coumarin, due to the spectral overlap between the emission spectrum of the coumarin subunit and the absorption spectrum

of the corrole moiety. *In vitro* experiments showed that corrole-coumarin dyads exhibited significant photodynamic anticancer activity toward all tested tumor cell lines. Further mechanistic studies using the SiHa cell line revealed that the absorbed **2-Ga** was extensively distributed in the cytoplasm and the nuclei. After PDT treatment, **2-Ga** induced tumor cell S phase arrest, ROS level increase and mitochondrial membrane potential destruction, which finally led to the apoptosis of SiHa cells.

Acknowledgments

This work was supported by the National Natural Science Foundation of China (Nos. 21671068, 81400023), the National Basic Research Program (973 Program) of China under Grant 2013CB922403 and the Open Fund of State Key Laboratory of Optoelectronic Materials and Technologies (Sun Yat-Sen University) (No. OEMT-2015-KF-05).

Supporting information

Figures S1–S20 are given in the supplementary material. This material is available free of charge *via* the Internet at http://www.worldscinet.com/jpp/jpp.shtml.

REFERENCES

1. Giribabu L, Sudhakar K, Sabapathi G and Kanaparthi RK. *J. Photochem. Photobiol., A* 2014; **284**: 18–26.
2. Nikodem C, Agnieszka N-K, Daniel TG and Sebastian M. *Phys. Scr.* 2013; **2013**: 014009-1–014009-4.
3. Fischer S, Vestfrid J, Mahammed A, Herrmann — Westendorf F, Schulz M, Müller J, Kiesewetter O, Dietzek B, Gross Z and Presselt M. *ChemPlusChem* 2016; **81**: 594–603.
4. Hwang JY, Lubow J, Chu D, Ma J, Agadjanian H, Sims J, Gray HB, Gross Z, Farkas DL and Medina-Kauwe LK. *Mol. Pharmaceutics* 2011; **8**: 2233–2243.
5. Zhang Z, Wang HH, Yu HJ, Xiong YZ, Zhang HT, Ji LN and Liu HY. *Dalton Trans.* 2017; **46**: 9481–9490.
6. Chen L, Hu TS and Yao ZJ. *Eur. J. Org. Chem.* 2008; **2008**: 6175–6182.
7. Jiao Y, Zhou L, He H, Yin J and Duan C. *Talanta* 2017; **162**: 403–407.
8. Kontogiorgis C, Detsi A and Hadjipavlou-Litina D. *Expert Opin. Ther. Pat.* 2012; **22**: 437–454.
9. Trenor SR, Shultz AR, Love BJ and Long TE. *Chem. Rev.* 2004; **104**: 3059–3078.
10. Cerqueira AFR, Almodôvar VAS, Neves MGPMS and Tomé AC. *Molecules* 2017; **22**: 1–26.
11. Lin WY, Long LL, Feng JB, Wang B and Guo CC. *European J. Org. Chem.* 2007; **2007**: 4301–4304.
12. Concellón A, Marcos M, Romero P, Serrano JL, Termine R and Golemme A. *Angew. Chem., Int. Ed.* 2017; **56**: 1259–1263.
13. Tasior M, Gryko DT, Pielacińska DJ, Zanelli A and Flamigni L. *Chem. —Asian J.* 2010; **5**: 130–140.
14. Mao M and Song QH. *Dyes Pigments* 2012; **92**: 975–981.
15. Cao XW, Lin WY and Yu QX. *J. Org. Chem.* 2011; **76**: 7423–7430.
16. Santos CIM, Oliveira E, Menezes JCJMDS, Barata JFB, Faustino MAF, Ferreira VF, Cavaleiro JAS, Neves MGPMS and Lodeiro C. *Tetrahedron* 2014; **70**: 3361–3370.
17. Zhou XQ, Meng LB, Huang Q, Li J, Zheng K, Zhang FL, Liu JY and Xue JP. *ChemMedChem* 2015; **10**: 304–311.
18. Hania PR, Heijs DJ, Bowden T, Pugžlys A, van Esch J, Knoester J and Duppen K. *J. Phys. Chem. B* 2004; **108**: 71–81.
19. Singh DK and Nath M. *Dyes Pigm.* 2015; **121**: 256–264.
20. Singh DK and Nath M. *RSC Adv.* 2015; **5**: 68209–68217.
21. Dichtel WR, Hecht S and Fréchet JMJ. *Org. Lett.* 2005; **7**: 4451–4454.
22. Tasior M, Voloshchuk R, Poronik YM, Rowicki T and Gryko DT. *J. Porphyrins Phthalocyanines* 2011; **15**: 1011–1023.
23. Bursa B, Barszcz B, Bednarski W, Lewtak JP, Koszelewski D, Vakuliuk O, Gryko DT and Wrobel D. *Phys. Chem. Chem. Phys.* 2015; **17**: 7411–7423.
24. Ding T, Aleman EA, Modarelli DA and Ziegler CJ. *J. Phys. Chem. A* 2005; **109**: 7411–7417.
25. Weaver JJ, Sorasaenee K, Sheikh M, Goldschmidt R, Tkachenko E, Gross Z and Gray HB. *J. Porphyrins Phthalocyanines* 2004; **8**: 76–81.
26. Tasior M, Deperasinska I, Morawska K, Banasiewicz M, Vakuliuk O, Kozankiewicz B and Gryko DT. *Phys. Chem. Chem. Phys.* 2014; **16**: 18268–18275.
27. Shao WL, Wang H, He S, Shi L, Peng KM, Lin YF, Zhang L, Ji LN and Liu HY. *J. Phys. Chem. B* 2012; **116**: 14228–14234.
28. Brisach-Wittmeyer A, Lobstein S, Gross M and Giraudeau A. *J. Electroanal. Chem.* 2005; **576**: 129–137.
29. An BJ, Wang B, Hu JH, Xu SY, Huang L, Li XS and Chan ASC. *J. Med. Chem.* 2018; **61**: 2571–2588.
30. Zhang C, Han BJ, Zeng CC, Lai SH, Li W, Tang B, Wan D, Jiang GB and Liu YJ. *J. Inorg. Biochem.* 2016; **157**: 62–72.
31. Seybold PG and Gouterman M. *J. Mol. Spectrosc.* 1969; **31**: 1–13.
32. Frisch MJ, Trucks GW, Schlegel HB, Scuseria GE, Robb MA, Cheeseman JR, Scalmani G, Barone V, Mennucci B, Petersson GA, Nakatsuji H, Caricato M, Li X, Hratchian HP, Izmaylov AF, Bloino J,

Zheng G, Sonnenberg JL, Hada M, Ehara M, Toyota K, Fukuda R, Hasegawa J, Ishida M, Nakajima T, Honda Y, Kitao O, Nakai H, Vreven T, Montgomery JA, Jr., Peralta JE, Ogliaro F, Bearpark M, Heyd JJ, Brothers E, Kudin KN, Staroverov VN, Kobayashi R, Normand J, Raghavachari K, Rendell A, Burant JC, Iyengar SS, Tomasi J, Cossi M, Rega N, Millam JM, Klene M, Knox JE, Cross JB, Bakken V, Adamo C, Jaramillo J, Gomperts R, Stratmann RE, Yazyev O, Austin AJ, Cammi R, Pomelli C, Ochterski JW, Martin RL, Morokuma K, Zakrzewski VG, Voth GA, Salvador P, Dannenberg JJ, Dapprich S, Daniels AD, Farkas O, Foresman JB, Ortiz JV, Cioslowski J and Fox DJ. Gaussian, Inc., Wallingford CT, 2009.

33. Bendix J, Dmochowski IJ, Gray HB, Mahammed A, Simkhovich L and Gross Z. *Angew. Chem., Int. Ed.* 2000; **39**: 4048–4051.
34. Gryko DT and Koszarna B. *Org. Biomol. Chem.* 2003; **1**: 350–357.
35. Littler BJ, Miller MA, Hung C-H, Wagner RW, O'Shea DF, Boyle PD and Lindsey JS. *J. Org. Chem.* 1999; **64**: 1391–1396.